BISTATIC RADAR SCATTERING AND POLARIZATION PROPERTIES OF THE ARISTARCHUS AND TAURUS-LITTROW PYROCLASTIC DEPOSITS. L. M. Carter[1], G. W. Patterson[2], C. D. Neish[3], B. J. Thomson[4], J. T. Cahill[2] and the Mini-RF Team [1]Lunar and Planetary Laboratory, University of Arizona (lmcarter@email.arizona.edu), [2]Johns Hopkins University Applied Physics Laboratory, [3]The University of Western Ontario, [4]University of Tennessee.

Introduction: There are many outstanding questions about the large lunar pyroclastic deposits. Most of these deposits (hundreds to tens of km^2 in size) are thought to have formed in periods of fire fountaining during the time of emplacement of the mare basalts. Prior work has suggested that these deposits may vary in composition and glass abundance [1,2,3,4], perhaps originating from different depths or source regions. However, the compositions of many of the deposits are still poorly constrained. In addition, it is difficult to assess the thickness and volume of the pyroclastics, which may range from a regolith component in some places to tens-of-meter thick deposits in others. Prior radar observations have revealed that the deposits likely vary significantly in thickness and embedded rock abundance, and in the case of Aristarchus there are clearly variations across the deposit [5,6]. Radar data have led to the possible identification of other large pyroclastics [6], such as the Tacquet formation and radar-dark deposits in Mare Nubium [7] based on low circular polarization ratio values.

Bistatic observations using the Mini-RF radar on Lunar Reconnaissance Orbiter provide a new opportunity to investigate the properties of these deposits. The dielectric constant of the pyroclastic deposits depends on their composition and density, and radar data acquired with differing viewing geometries can place additional constraints on quantitative models of the surface and subsurface structure. We are currently working to obtain bistatic data for large lunar pyroclastic deposits with the aim of comparing the radar properties (backscatter power and polarimetry) across deposits and in some cases modeling to obtain dielectric constants.

Data Sets: The ability to acquire bistatic radar data using Mini-RF [8] presents an opportunity to experiment with the transmitted signal and observe the resulting scattering function. These data can place additional constraints on the structure (roughness) and dielectric properties of the lunar surface beyond what can be learned with monostatic data (i.e. when the transmitter and receiver are co-located). Mini-RF has acquired the largest such planetary dataset, and the tracks cross a variety of different terrain types and at both X-band (λ=4.2 cm) and S-band (λ=12.6 cm) frequencies. These data are spatially averaged to produce 100 m/pixel resolution images, with around 40 looks. The exact resolution and data characteristics vary depending on the geometry of the individual collect. To date, Mini-RF has collected bistatic data across the Aristarchus and Taurus-Littrow large pyroclastic deposits.

In addition to the normally acquired bistatic data, we acquired one data track across the Aristarchus pyroclastic deposit where the incidence angle and emission angle (between nadir and the observer direction) were identical (Fig. 1). This geometry has been used for bistatic observations before [9,10,11], and it has the advantage of capturing the specular reflection, which can then be used to derive permittivity via the reflection coefficient. In fact, most radar bistatic observations prior to Mini-RF were acquired this way, using the spacecraft as transmitter and receiving with a ground station. In the Mini-RF case, we transmit from the ground station and receive using the spacecraft. This particular forward scattering geometry is not useful for image formation as there are extensive ambiguities; however, the data can be summed along a track on the surface to determine the relative level of backscatter at the specular point.

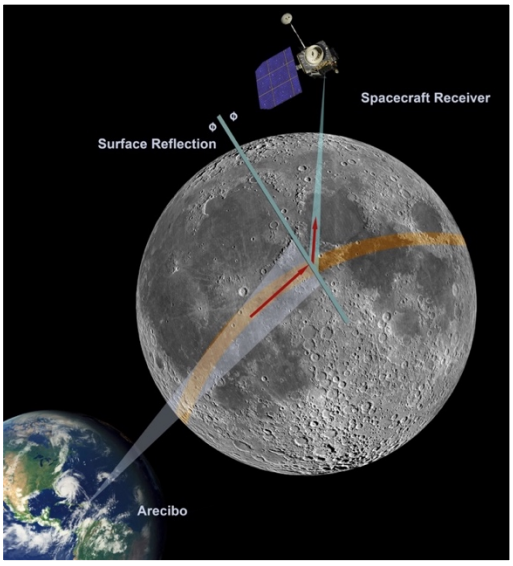

Fig. 1: An illustration of the forward scattering observation geometry where the incidence and emission angles were identical. Mini-RF has obtained one such observation, to date, for a location near the center of the Aristarchus pyroclastic deposit. These data can be modeled to derive the permittivity at the target region. Credit: NASA GSFC/J. Friedlander.

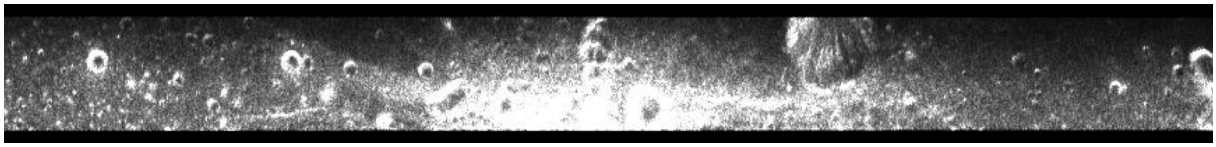

Fig. 3: The center portion of a Mini-RF bistatic X-band image of the Taurus-Littrow pyroclastic deposit (total power image, LXT_37221). For this dataset, the bistatic angle is 4.62° and the central incidence angle is 39 degrees. This data track crosses the central part of the pyroclastic to the west of the crater Clerke. The center area (Catena Littrow) is brighter due to rough rocky terrain and steep crater walls at low incidence angles.

Aristarchus: Aristarchus, the largest pyroclastic deposit, was one of the first targets imaged with Mini-RF (at S-band) and the bistatic data are analyzed in [8]. We will present the data set that was acquired using a forward scattering collect in May 2014 for purposes of deriving permittivity values (Fig. 2). This data set was acquired in the central part of the deposit where there are thought to be relatively thick deposits [5]. Due to the need for precise backscatter measurements for this technique [10], processing of this particular data set was delayed while we explored the effects of the onboard compression algorithm on the data [12]. Now that those effects are understood we are returning to the efforts to derive permittivities.

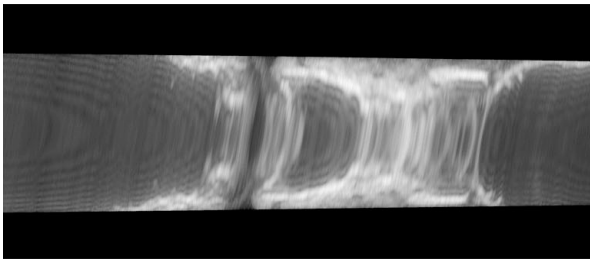

Fig. 2: Data from a forward scatter collect across the Aristarchus pyroclastic deposit, presented as an image. Bright echoes are apparent at the center of the image as the radar passes through the specular point, but imaging is not possible with this geometry.

Taurus-Littrow: Taurus-Littrow is one of the largest pyroclastic deposits and has a possible ground-truth analog from the Apollo 17 landing site. Two data strips were acquired at X-band with bistatic angles of 0.97 and 4.62 and incidence angles of 31° and 39°. One of the tracks covers the central area of the pyroclastics, just west of Clerke crater and including part of Rimae Littrow (Fig. 3). A second track lies to the west near the southwest part of the mapped deposit. With a shorter wavelength sensitive to smaller (cm-sized) rocks, the X-band data is expected to appear brighter and have larger circular polarization ratio (CPR) values than the corresponding S-band data, particularly in regions with significant crater ejecta. We will compare these data with Mini-RF monostatic data as well as with longer wavelength S-band data.

Future Work: The Mini-RF team is currently seeking to acquire bistatic data of additional targets and we will present the latest plans. In particular, we would like to image Sinus Aestuum where spinel deposits have been identified [2], as well as the radar-dark, low CPR regions in Mare Serenitatis (Tacquet Formation) and Mare Nubium that could be large pyroclastic deposits but could also be mare flows with unusual low CPR values. In these cases, it is especially important to determine the near-surface characteristics of the terrain to determine whether there is mantling by pyroclastics.

These acquisitions require significant advance planning between the LRO operations team and ground-based facilities, and the collects are therefore limited to around a couple per month. However, the usefulness of these datasets increases greatly as more are obtained and can be compared to one another and to monostatic data. As LRO moves toward future extended missions, it is important to continue the efforts to collect as many different bistatic data sets as can reasonably be obtained so that the science derived from the data can be maximized.

References: [1] Gaddis et al., Icarus, 161, 262, 2003. [2] Sunshine et al., LPSC 45, abstract 2297, 2014. [3] Jawin et al., JGR, 120, 1310, 2015. [4] Trang et al., Icarus, 283, 232, 2017. [5] Campbell et al., Geology, 36, 135, 2008. [6] Carter et al., JGR, 114, E11004, doi:10.1029/2009JE0034062009. [7] Carter et al., LPSC 48, abstract 1736, 2017. [8] Patterson et al., Icarus, 283, 2, 2017. [9] Ford et al., Science, 272, 1628, 1996. [10] Simpson et al., Proc IEEE, 99, 858, 2011. [11] Marouf et al., AAS DPS meeting #48, abstract 412.02, 2016. [12] Carter et al., IEEE Trans. Geosci. Rem. Sens., 55, 1915, 2017.

Additional Information: This work was supported through LRO Mini-RF funds to L. M. Carter.